ACS NANO

www.acsnano.org

ARTICLE

Enhanced Diffusive Transport in Fluctuating Porous Media

Raphaël Sarfati, Christopher P. Calderon, and Daniel K. Schwartz*

Cite This: *ACS Nano* 2021, 15, 7392–7398

Read Online

ACCESS | Metrics & More | Article Recommendations | Supporting Information

ABSTRACT: **Mass transport within porous structures is a ubiquitous process in biological, geological, and technological systems. Despite the importance of these phenomena, there is no comprehensive theory that describes the complex and diverse transport behavior within porous environments. While the porous matrix itself is generally considered a static and passive participant, many porous environments are in fact dynamic, with fluctuating walls, pores that open and close, and dynamically changing cross-links. While diffusion has been measured in fluctuating structures, notably in model biological systems, it is rarely possible to isolate the effect of fluctuations because of the absence of control experiments involving an identical static counterpart, and it is generally impossible to observe the dynamics of the structure. Here we present a direct comparison of the diffusion of nanoparticles of various sizes within a trackable, fluctuating porous matrix and a geometrically equivalent static matrix, in conditions spanning a range of regimes from *obstructed* to *highly confined*. The experimental system comprised a close-packed layer of colloidal spheres that were either immobilized to a planar surface or allowed to fluctuate locally, within the space defined by their nearest neighbors. Interestingly, the effective long-time diffusion coefficient was approximately 35−65% greater in the fluctuating porous matrix than in the static one (depending on the size of the nanoparticle probes), regardless of the geometric regime. This was explained by considering the enhancing effects of matrix fluctuations on the short-time diffusion coefficient and cooperative "gate-opening" motions of matrix particles and nanoparticle probes.**

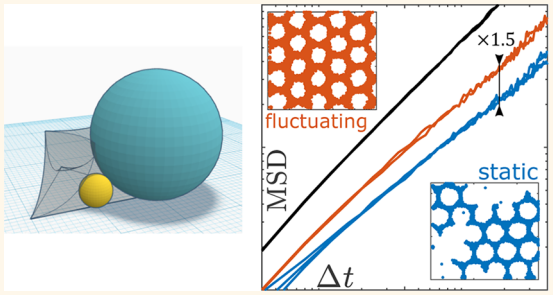

KEYWORDS: *porous media, fluctuations, diffusive transport, obstructed diffusion, confined diffusion, hydrodynamic coupling*

Biological, geological, and industrial processes frequently involve complex and tortuous high surface area environments. For example, transport of molecular and particulate species (heavy metals, pesticides, microbes, colloids, *etc.*) within the fractured and granular Earth subsurface is critical to many processes associated with water treatment, environmental remediation, and energy production.[1,2] Transport of most biomolecular species takes place within the crowded and porous environments inside cells or tissues. And while high surface area materials are prized for their ability to enhance technological processes involving chemical reactions and separation or purification, transport within such materials remains an ongoing challenge to understand and optimize. Porous membranes used in water purification systems and filtration devices, for example, comprise a solid matrix embedding a percolated network of cavities, pores, and channels.[3,4] Diffusive dynamics in such structures can be challenging to describe, even qualitatively. For example, environments may range from a regime where species are merely obstructed—and transport is simply dominated by excluded volume effects—to the opposite extreme where species are strongly confined—and transport can be simplistically considered a sequential process of confinement within cavities punctuated by translocation through pores connecting neighboring cavities.

Materials engineering traditionally relies on the structure−function paradigm. In the context of porous materials, this implies that the matrix geometry and surface chemistry determine the transport properties of solutes and particles.[5] Within this framework, structure is implicitly assumed to represent a static or average property, although it has long been recognized that materials may fluctuate, rearrange, or evolve with time. Thus, while transport has been studied under the direction of various driving forces, including thermal motion (*i.e.*, diffusion), convective flow, and external fields, in most cases the porous matrix itself has simplistically been considered a static and passive participant, characterized sufficiently by its

Received: January 26, 2021
Accepted: March 29, 2021
Published: April 1, 2021

https://doi.org/10.1021/acsnano.1c00744
ACS Nano 2021, 15, 7392–7398

geometric properties. In recent years, there has been an increasing interest in developing theories to describe the effects of matrix heterogeneity and dynamics on transport, notably for the relevance to transport in biological environments.[6−8] The framework of "diffusing diffusivities",[9−11] which describes a time-evolving diffusion coefficient, provides an *ad hoc* theoretical basis to approach these questions, but is difficult to connect to physical properties of real systems. Due to the complexity of these systems, approaches have generally focused on a particular geometry, such as transport within a channel with fluctuating walls.[12−14] However, depending on the model employed, the results are often contradictory. For example, fluctuations of the porous environment have been predicted either to inhibit or to enhance the diffusion of particles within the pore space, depending on the assumptions employed in the theory. Consequently, a general understanding of the interplay between entropic and hydrodynamic effects remains incomplete, and experimental findings that could help refine these theories have been sparse. While a few studies have observed anomalous diffusion in model biological systems,[6,15] the exact effect of environmental fluctuations remains difficult to characterize notably due to the difficulty to observe these fluctuations and to compare with an appropriate static equivalent system. Here, we describe an experimental system that permits the direct comparison of transport within static and temporally fluctuating porous environments with the same average, periodically ordered structure. We find that self-diffusion of tracers of various sizes is significantly enhanced (by an average of 50%) by the presence of thermal fluctuations of the embedding matrix, compared to the static structure. These findings, interpreted using random walk simulations and statistical modeling (and in the context of existing theories), suggest that both hydrodynamic coupling and pore-opening contribute to enhanced transport.

In addition to its relevance to test and refine theoretical models, the experimental system described here, comprising a close-packed layer of colloidal spheres, either fluctuating or static, is a directly relevant experimental realization of important geological and industrial systems. For example, water-saturated soils, found between surface and subsurface waters, consist of packed loose sediments at the Brownian micrometer-scale (silt and clay). Transport of nanoparticles, macromolecules, viral particles, and microorganisms within these environments remains a major fundamental issue for environmental contamination and remediation. While soil column experiments measure macroscopic transport rates of pollutants, the underlying microscopic mechanisms are not well understood.[16,17] Moreover, many industrial filtration processes rely on transport through mesh-like polymer matrices consisting of cavities connected by pores (porous polymers formed *via* phase inversion, hydrogels, inverse opals, *etc.*), at scales where thermal fluctuations may be significant. Since these systems are designed with extremely specific and selective objectives,[18] properly accounting for fluctuations is crucial.

RESULTS AND DISCUSSION

We tracked the diffusive motion of fluorescent polystyrene tracer beads of radii ρ = 50, 100, 150, 200, and 250 nm confined between a flat surface and a close-packed layer of monodisperse silica spheres of radius R = 1 μm. This periodic porous void space consists of cavities (tetrahedron-like shape between three spheres) connected by channels (between two adjacent spheres). Depending on the preparation procedure (see Methods), the silica spheres either (1) attached slowly and irreversibly to the coverslip and remained immobile in a hexagonal configuration (static lattice) or (2) were free to move in the horizontal plane, but given the high packing density, rearrangements were impossible and the spheres fluctuated only about an average position in the crystalline arrangement (dynamic lattice). A double illumination technique was used to image and track simultaneously the silica spheres and the tracers within 1 μm from the coverslip (Figure 1a and SI Movies).

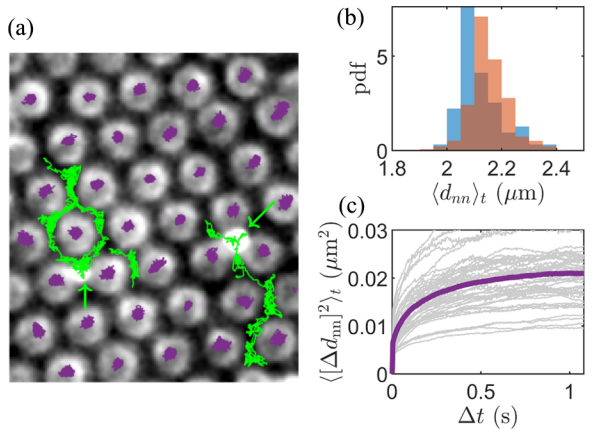

Figure 1. Experimental system. (a) Frame of an experimental movie, showing a close-packed layer of 1-μm-radius spheres, and two 200 nm tracers diffusing in the interstices between the bottom coverslip and the plane defined by the spheres' centers. The point-spread functions of tracers appear as bright, white disks indicated by green arrows; see also SI Movies. Spheres of the dynamic lattice are tracked by Hough transform, and the trajectories of the centroids are overlaid in purple; tracers are tracked by intensity detection, and representative trajectories are overlaid in green. Due to optical artifacts, lattice spheres appear smaller than their true size and may sometimes seem mutually connected (but they are not), and fluorescent tracers appear much larger than their actual size. (b) Distributions of time-averaged distances between nearest neighbors $\langle d_{nn}\rangle_t$ for a static lattice (blue) and a dynamic lattice (orange). The distribution overlap appears brown at the center. (c) Variances of d_{nn} at lag time Δt for a dynamic lattice (gray curves) and average of variances (purple).

The static and dynamic lattices have the same time-averaged geometry. In particular, the distributions of distances between nearest neighbors, d_{nn}, are strongly overlapping (Figure 1b), although dynamic lattices are very slightly larger on average. Depending on the specific field-of-view, a typical static lattice exhibits $\langle d_{nn}\rangle \simeq 2.10$ μm with a standard deviation of about $\sigma \simeq 0.08$ μm, while a typical dynamic lattice has $\langle d_{nn}\rangle \simeq 2.15$ μm and $\sigma \simeq 0.10$ μm, corresponding to an increase in average unit cell length of about 3%. The spheres in the dynamic lattice exhibit significant motion about their mean locations corresponding to confined Brownian motion, with fluctuations of nearest-neighbor distances d_{nn} on the order of 0.1 μm over time scales $\tau_S \approx 0.1$s (Figure 1c).

In comparing the diffusion of tracer particles within the static and dynamic lattices, the tracer trajectories apparently access a larger fraction of space in the dynamic lattice (Figure 2a,b), due to the motion of the matrix as fluctuations open and close different void spaces. To quantify transport, we calculate the 2D, ensemble-averaged mean-squared displacements

https://doi.org/10.1021/acsnano.1c00744
ACS Nano 2021, 15, 7392−7398

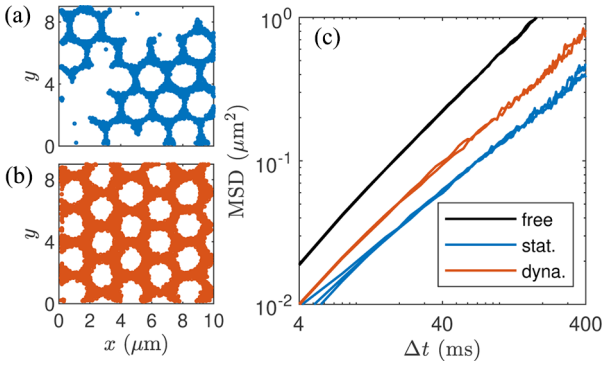

Figure 2. Results from experiments. (a, b) 2D projected trajectories of 200 nm tracers in a (a) static and (b) dynamic lattice. Transport in the static lattice shows less exploration, both locally (within channels and cavities) and globally (less cavities are visited). (c) Mean-squared displacements *vs* lag time for 150 nm tracers in the free solvent (black), within the static lattice (blue) and within the dynamic lattice (orange). Three experimental curves from different fields-of-view are shown for each condition. Representative curves for other tracer sizes are shown in the Supporting Information.

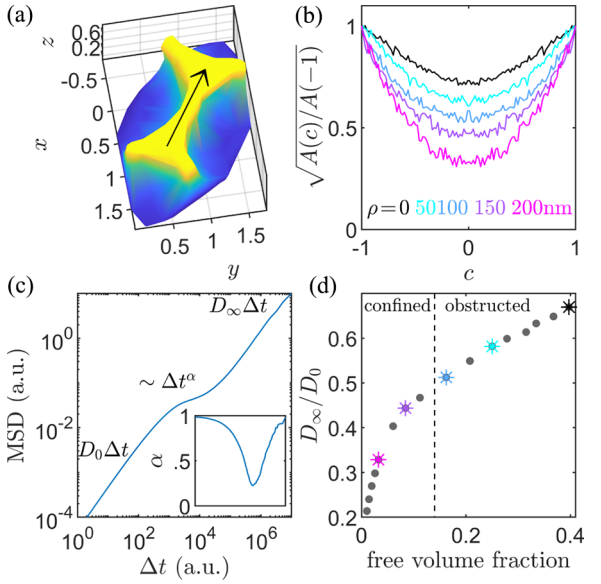

Figure 3. Results from kMC simulations. (a) Accessible volume within a lattice cell. (b) Relative change in cross-sectional length scale $\sqrt{A(c)/A(-1)}$ for tracers of different sizes on a path from the center of one cavity ($c = -1$) to the center of an adjacent cavity ($c = 1$) through a channel ($c = 0$), following the arrow in (a). $A(c)$ was calculated from Monte Carlo simulations. (c) Simulated MSD curve of a tracer of radius $0.24R$, showing two asymptotic regimes of normal Fickian diffusion (MSD $\sim \Delta t$) with different diffusion coefficients, D_0 and D_∞, separated by a regime of subdiffusion ($\alpha < 1$) at intermediate time scales. (Inset) Value of the subdiffusive exponent $\alpha = d\log(\text{MSD})/d\log(\Delta t)$. (d) Relative decrease in the diffusion coefficient at long time scales D_∞ compared to free diffusion coefficient D_0 as a function of accessible volume fraction. Results for tracer sizes used in experiments are marked with colored stars. Accessible volume fractions were calculated from Monte Carlo simulations.

(MSD) over time intervals Δt as $\text{MSD}(\Delta t) = \langle(\vec{r}_{t+\Delta t} - \vec{r}_t)^2\rangle$, where $\vec{r}_t = (x_t\ y_t)$. As expected, compared to free diffusion in the unconfined fluid, long-time transport within the porous lattice is markedly hindered (Figure 2c) and also slowed at short times due to hydrodynamic friction in the confined environment. Importantly, transport is significantly enhanced in the dynamic lattice compared to the static lattice, at all resolvable time scales (down to $\Delta t = 4$ ms), with mean-squared displacements increasing by an average factor of approximately 1.5, depending on the size of the tracer particles. This dramatic and previously unreported enhancement of diffusion due to thermal fluctuation of the porous matrix is a major finding of this paper.

In order to understand the diffusion enhancement, we characterized the static lattice and transport within, using kinetic Monte Carlo (kMC) simulations and statistical modeling of trajectories. The unit cell of the periodic void space is shown in Figure 3a; however, the accessible volume depends on the size of the tracer. For lattice spheres of radius R, geometrical considerations show that the maximum tracer radius to fit through a channel is $R/4$ (250 nm in our experiments). For tracers much smaller than this, confinement is minimal, and transport can be considered *obstructed*, where the diffusion coefficient is reduced due simply to excluded volume effects. However, for larger tracer particles, diffusive transport is *confined* and qualitatively involves a sequential process of transient cavity confinement alternating with hops between adjacent cavities. In particular, for a tracer of radius ρ on a path defined by the coordinate c along a channel between the centers of adjacent cavities, the cross-sectional area $A(c)$ of accessible volume along c depends strongly on ρ. Figure 3b shows that the relative shrinking of $\sqrt{A(c)}$ between the cavity and the narrowest part of the channel ($c = 0$) is about 20% for 50 nm tracers and over 60% for 200 nm tracers. Therefore, as tracer size increases, hopping between cavities becomes more and more hindered.

We simulated random walks of tracer beads ($\rho < R/4$) within the void space defined by close-packed spheres and characterized the time-averaged excursions. For sufficiently large tracers, the MSD exhibits conventional cage dynamics, with linear behavior at short and long lag times, separated by an intermediate subdiffusive regime. The two asymptotic regimes are readily seen in the time dependence of the diffusive exponent α defined as $\text{MSD} \sim \Delta t^\alpha$ (Figure 3c and inset). At short time scales, the tracer is freely diffusive in a viscous fluid without perturbations from obstacles, so that $\alpha = 1$ (normal diffusion). At long time scales, the tracer has hopped between cavities a large number of times, so that diffusion is again normal. At intermediate time scales, diffusion is hindered by obstacles and the tracer bounces off of the confining surfaces, so that its dynamics is subdiffusive, $\alpha < 1$. This general behavior is commonly observed in corrugated environments.[14,19,20] The exact Δt-dependence of α depends on the specific geometry of the system.

Importantly, the effective diffusion coefficients (MSD/$4\Delta t$) at short and long time scales, D_0 and D_∞, respectively, are different, as long-time transport is defined by the ability of the tracer to move across the lattice, which is limited by obstacles and constrictions. In particular, with increasing tracer size, one expects a continuous transition to occur between obstructed diffusion and confined diffusion with a possibility of escape. For obstructed diffusion, D_∞ scales with accessible volume fraction ν_a,[21] as visible in Figure 3d for $\nu_a \gtrsim 0.17$. For confined diffusion, D_∞ depends on the time scale required to escape a cavity, which depends on the relative channel size. Intuitively,

https://doi.org/10.1021/acsnano.1c00744
ACS Nano 2021, 15, 7392−7398

D_∞ is expected to scale with L^2/τ, where L is the characteristic distance between neighboring cavities (here, $L = 2R$), and τ is the characteristic time delay between hops, *i.e.*, the typical cavity escape time. The transition between the two regimes occurs when the scaling of D_∞ with ν_a deviates from the obstructed diffusion behavior, which corresponds to tracer particles with approximately ρ = 100−150 nm, according to the simulation results in Figure 3d.

In experiments, fluctuation-induced diffusivity enhancement, by an average factor of approximately 1.5 ± 0.15, is observed for all tested tracer sizes, whether the tracer is much smaller than or of comparable size as the static channel size (Figure 4a). While there are modest apparent differences in the enhancement factors for different tracer particle sizes, there is no obvious trend, and all of the enhancements are much larger than what could be expected from slight differences in average lattice size, which could only account for up to a 10% increase (Supporting Information). Therefore, the results of the kMC simulations allow us to conclude that substantial tracer particle diffusion enhancement due to matrix fluctuations is observed in both obstructed and confined diffusion regimes. The fact that diffusion is enhanced in the obstructed regime, in which free diffusion is primarily inhibited by accessible volume effects and hydrodynamic friction, suggests that fluctuations of the matrix enhance the intrinsic short-time diffusion coefficient D_0, relative to that within a static lattice, perhaps by hydrodynamic coupling. Below, statistical modeling of trajectories is performed to test this hypothesis directly.

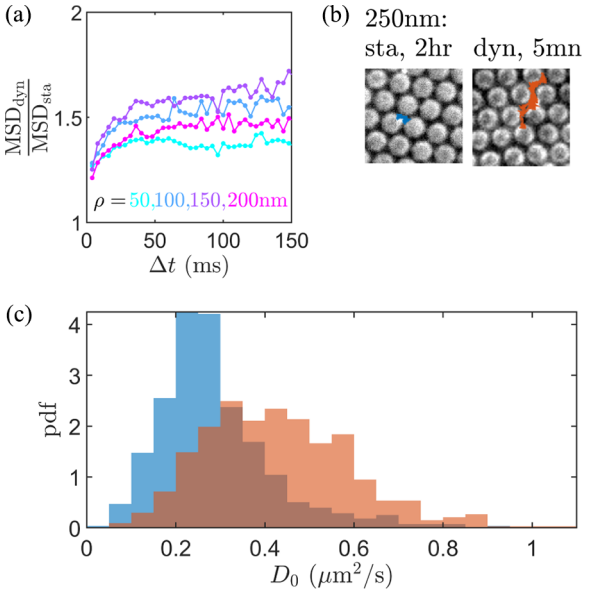

Figure 4. (a) Ratio of tracer MSD in the dynamic lattice (dyn) to tracer MSD in the static lattice (sta) *vs* lag time, averaged over several measurements. (b) Trajectories of a 250 nm ($R/4$) tracer, both in a static lattice (over 2 h) and in the dynamic lattice (over 5 min). (c) Distributions of effective short-term diffusion coefficients D_0 of 200 nm tracers in the static (blue) and dynamic (orange) lattices determined using statistical modeling of trajectories.

However, in the opposite strongly confined limit, where ρ approaches the theoretical channel size limit of $R/4$, macroscopic diffusion within static matrices becomes completely inhibited, and we hypothesize that an additional effect must be present. If one considers a tracer slightly too large to fit between two lattice spheres, $\rho = R/4 + \epsilon$, it can never escape a cavity in a static lattice. However, in a dynamic lattice, if fluctuations are larger than ϵ, there will be time intervals when the channel size is large enough to permit the tracer to escape. Indeed, in our experiments, 250 nm tracers never escape static cavities over experimental times of up to 4 h (Figure 4b), most likely due to short-range electrostatic repulsion, which reduces effective channel sizes.[20,22] However, the same tracers escape fluctuating cavities frequently (Figure 4b). For convenience, we refer to this as a "gate-opening" mechanism. This mechanism was observed in a similar glassy system with forced motion of the probes in ref 23 and is discussed rigorously in ref 14. When fluctuations follow a Ornstein−Ulenhbeck process (normally distributed excursions around an average value), it is found that long-time diffusivity is increased compared to static pores. But diffusivity enhancements vanish when tracers become much smaller than the average pore size, as intuitively expected.

These combined observations, in the small and large tracer particle size limits, suggest that D_∞ in fluctuating matrices is facilitated both by the enhancement of D_0 and by gate-opening, and it is interesting to understand the interplay of these mechanisms for intermediate tracer particle sizes. Conceptually, cavity escape is sometimes decomposed into two elementary processes, searching and translocation, and the escape time may be limited by either of these processes.[24] The searching process refers to random motion within the cavity that ends when the particle encounters an exit; the time associated with searching is therefore related to the short-time diffusion coefficient and geometric parameters such as accessible cavity volume. The translocation process accounts for the fact that there may be additional barriers to cavity escape—energetic (*e.g.*, electrostatic) or entropic (*e.g.*, steric)—and the translocation time may be related to the channel size or, in this case, fluctuations.

To understand the dominant source of enhanced diffusion in the confined regime, we performed a detailed analysis of the trajectories of 200 nm tracer particles using a statistical modeling approach developed in ref 25, where trajectories were modeled as a successive series of Ornstein−Uhlenbeck processes whose harmonic potential strength and centers, or "trap locations", were implied by the observed data. A maximum-likelihood estimation approach was used to extract the apparent short-time diffusivity and harmonic potential parameters associated with each trap from experimental trajectories by decoupling actual particle fluctuations from experimental measurement artifacts such as motion blur and localization error induced by point-spread function estimation. This analysis found that differences in the estimated effective trap potential strengths were not statistically significant for trajectories in the static and dynamic matrices. This suggested that the effective restoring forces in the cavity did not change and that enhanced cavity escape was not due to a reduction of the effective cavity accessible volume. Importantly, the modeling indicated that the effective local diffusion coefficients, D_0, are significantly larger in dynamic cavities than in static ones. Figure 4c shows representative distributions of local diffusion coefficients associated with trajectories in equivalent static and dynamic cavities. Combined, these observations suggest that the dominant mechanism responsible for the enhancement of diffusion in the majority of dynamic matrices involves the increase of local diffusive mobility within cavities, presumably due to hydrodynamic coupling with the

https://doi.org/10.1021/acsnano.1c00744
ACS Nano 2021, 15, 7392−7398

fluctuating matrix particles, which enhances the search for cavity exits. It appears that the gate-opening mechanism becomes significant only in the asymptotic limit as ρ approaches $R/4$, where translocation is completely restricted in static environments.

Theoretical predictions of the effects of matrix fluctuations on particle diffusion are limited and provide mixed guidance. Of course, it is well established that hydrodynamic coupling/friction between a static surface and a nearby diffusing particle hinders Brownian mobility[21,26] and that this impacts transport in a tortuous and heterogeneous environment.[27,28] Notably, this explains why short-time diffusion is slower within both static and dynamic porous environments compared to free liquid (Figure 2c) and also why our experimentally measured D_∞ values are smaller than expected from simulations, which include only (geometrical) confinement but no hydrodynamic interactions (SI). The effect of viscous friction is more pronounced for larger tracers (notably larger than 50 nm), since their surfaces are closer to no-slip boundaries within the porous medium on average. However, when the surrounding surfaces exhibit thermal fluctuations, local diffusion of nanoparticles is significantly enhanced, which has not previously been observed. This cannot simply be explained using pairwise hydrodynamic interactions between the tracer and the spheres that comprise the matrix (SI), since the hydrodynamic effects intrinsically involve multibody effects,[29] and perhaps even correlations between pore opening and outward flow. While no comprehensive theory currently exists to describe such phenomena, this could be fertile ground for future theoretical development.

It seems clear that hydrodynamic coupling must be explicitly considered to explain our findings. For example, for large channels where hydrodynamic effects can be neglected, thermal fluctuations of the walls are believed to decrease diffusive rates.[12] In a more general case where both hydrodynamic coupling and entropic trapping are taken into account, hindering or enhancement of short-time local diffusion might depend on the spectrum and amplitude of fluctuations. Recently, a model was proposed by Marbach *et al.* that accounts for both geometrical effects and hydrodynamic interactions within a fluctuating structure. Following this model, we have performed a semiquantitative analysis of our experimental system. For a channel with average height H and spatiotemporal fluctuations $h(x, t)$, in the obstructed regime where $|\tilde{h}| \ll 1$ ($\tilde{h} = h/H$) with a single wave vector κ, the model of ref 13 finds an effective diffusion coefficient relative to average diffusivity in the fluid $D_e/\bar{D} = 1 - Z_t \cdot \langle \tilde{h}^2 \rangle$, where

$$Z_t = \int \frac{(\bar{D}\kappa^2)^2 - 3\omega^2}{(\bar{D}\kappa^2)^2 + \omega^2} S(\omega)\, d\omega \quad (1)$$

$S(\omega)$ is the spectrum of temporal fluctuations and $\bar{D}$ the value of the diffusion coefficient in the fluid, when *static* hydrodynamic interactions are taken into account. Consequently,

$$\Delta D_e = D_e^{dyn} - D_e^{sta} = \bar{D}\langle \tilde{h}^2 \rangle (Z_t^{sta} - Z_t^{dyn}) \quad (2)$$

For a static channel, $S(\omega) = \delta(\omega)$, so that $Z_t^{sta} = 1$. When thermal fluctuations of relative amplitude λ are added to the static profile, $S(\omega) = \delta(\omega) + \lambda^2 R(\omega)$. If these fluctuations are described by an Ornstein–Uhlenbeck process (confined diffusion) with a Lorentzian spectrum $R(\omega) \sim (1 + \tau_S^2\omega^2)^{-1}$, then $1 - Z_t^{dyn} \sim (3 - D\bar{\kappa}^2\tau_S)/(D\bar{\kappa}^2\tau_S + 1)$, with τ_S the time scale of fluctuations of the pores (*i.e.*, spheres). From our experimental measurements, $\bar{D} \simeq 10^{-13}$ m^2/s (Figure 4c), $\kappa = 2\pi/(2R)$, $\tau_S \simeq 0.1$ s (Figure 1c), so that $D\bar{\kappa}^2\tau_S \ll 1$. Hence $1 - Z_t^{dyn} > 0$, and $\Delta D_e > 0$. Therefore, this theoretical framework indeed predicts that diffusion will be enhanced in this regime of fluctuations relative to the static equivalent, as observed in our experiments. Since the geometry explored by this theory is not the same as that of our experiments, we limit this comparison to a qualitative discussion.

CONCLUSIONS

Our experimental findings, elucidated by kinetic Monte Carlo simulations and statistical trajectory modeling, show that equilibrium thermal fluctuations within a submicron-scale porous environment result in significantly enhanced diffusion of tracer particles at both short and long time scales, compared to diffusion within a geometrically equivalent porous matrix. Importantly, these results hold both for the obstructed diffusion regime, where the main effect is presumably due to the hydrodynamic coupling to flow resulting from matrix fluctuations, and in the confined diffusion regime, where pore opening also facilitates escape. Since the diffusion enhancement is substantial, with typical increases in the range of 50%, we hope that these findings will stimulate further experimental, theoretical, and computational studies to provide a comprehensive understanding of the various roles of temporal fluctuations for transport in confined and porous structures. In particular, the results presented in this paper clearly point to the need to include hydrodynamic coupling in appropriate models. Future experiments should also attempt to correlate tracer escape with cavity size fluctuations to further understand the pore-opening mechanism. Currently, the localization uncertainty of the lattice spheres is too large, and the time resolution insufficient, to rigorously correlate both dynamics. An improved experimental setup could circumvent this obstacle.

More broadly, since fluctuations can have such a dramatic effect on transport, this suggests opportunities to influence transport by controlling the dynamic properties of the porous matrix, in addition to its average structural properties. In fact, one can imagine replacing the traditional structure–function paradigm with an updated structure-dynamics-function version, which could lead to materials with the potential to break traditional scaling limitations, such as the permeability–selectivity trade-off, and reduce the propensity to foul.[3] Considering temporally fluctuating systems may provide an alternative avenue to go beyond material-based solutions for industrial applications. Possibly, designing porous systems that can be switched between a static state and a dynamic state[30] could allow increasing transport rate and decreasing irreversible degradation.

METHODS

Upon immersion in deionized water, 1-μm-radius silica spheres (Corpuscular Inc., CV < 2%) quickly sediment toward the bottom coverslip of a closed 10 μL microscope chamber (Grace Bio-Laboratories CoverWell) and spontaneously self-assemble in hexagonal packing. Short-range electrostatic repulsion maintains the spheres slightly apart. To create the static lattice, the coverslip was pretreated by illumination under UV light for over 1 h, so that the silica spheres bind slowly and irreversibly to it after sedimenting. The sample was then dried and passivated by contact with ambient air for over 24 h. A solution of fluorescent tracers (Thermo Scientific FluoroMax, CV < 5%) was injected to the dried sample before starting experiments. To create the dynamic lattice, a mixture of silica spheres

https://doi.org/10.1021/acsnano.1c00744
ACS Nano 2021, 15, 7392–7398

and tracers was deposited on an untreated coverslip. A double illumination technique is used to image tracers and spheres simultaneously: bright-field illumination reveals silica spheres by light scattering, and monochromatic illumination at high incident angle excites fluorescent emission from tracers only within about 1 μm from the coverslip. We used a Nikon TE inverted microscope with 150× magnification for imaging, and standard tracking algorithms were employed to extract trajectories.[31]

ASSOCIATED CONTENT

Supporting Information

The Supporting Information is available free of charge at https://pubs.acs.org/doi/10.1021/acsnano.1c00744.

Supporting movie showing experimental data of tracer diffusion in the static lattices (AVI)

Supporting movie showing experimental data of tracer diffusion in the dynamic lattices (AVI)

Additional MSD curves (Figure S1), supporting data relative to the influence of lattice size (Figure S2) and hydrodynamic effects (Figure S3) on long-time diffusion coefficients, and a discussion on many-body effects in fluctuating cavities (PDF)

AUTHOR INFORMATION

Corresponding Author

Daniel K. Schwartz − *Chemical and Biological Engineering Department, University of Colorado, Boulder, Colorado 80303, United States;* orcid.org/0000-0001-5397-7200; Email: daniel.schwartz@colorado.edu

Authors

Raphaël Sarfati − *Chemical and Biological Engineering Department, University of Colorado, Boulder, Colorado 80303, United States;* orcid.org/0000-0003-4944-0632

Christopher P. Calderon − *Chemical and Biological Engineering Department, University of Colorado, Boulder, Colorado 80303, United States; Ursa Analytics, Inc., Denver, Colorado 80212, United States*

Complete contact information is available at: https://pubs.acs.org/10.1021/acsnano.1c00744

Notes

The authors declare no competing financial interest.

ACKNOWLEDGMENTS

Primary support for this research was provided by the U.S. Department of Energy, Office of Science, Basic Energy Sciences (award #DE-SC0001854). We thank Sophie Marbach and Eric Dufresne for helpful conversations.

REFERENCES

(1) McGechan, M.; Lewis, D. SW—Soil and Water: Transport of Particulate and Colloid-Sorbed Contaminants through Soil, Part 1: General Principles. *Biosystems Engineering* **2002**, *83*, 255−273.

(2) McCarthy, J. F.; McKay, L. D. Colloid Transport in the Subsurface: Past, Present, and Future Challenges. *Vadose Zone J.* **2004**, *3*, 326−337.

(3) Werber, J. R.; Osuji, C. O.; Elimelech, M. Materials for Next-Generation Desalination and Water Purification Membranes. *Nature Reviews Materials* **2016**, *1*, 16018.

(4) Park, H. B.; Kamcev, J.; Robeson, L. M.; Elimelech, M.; Freeman, B. D. Maximizing the Right Stuff: The Trade-Off between Membrane Permeability and Selectivity. *Science* **2017**, *356*, No. eaab0530.

(5) Das, S.; Heasman, P.; Ben, T.; Qiu, S. Porous Organic Materials: Strategic Design and Structure−Function Correlation. *Chem. Rev.* **2017**, *117*, 1515−1563. PMID: 28035812.

(6) Wang, B.; Anthony, S. M.; Bae, S. C.; Granick, S. Anomalous Yet Brownian. *Proc. Natl. Acad. Sci. U. S. A.* **2009**, *106*, 15160−15164.

(7) Weigel, A. V.; Simon, B.; Tamkun, M. M.; Krapf, D. Ergodic and Nonergodic Processes Coexist in the Plasma Membrane as Observed by Single-Molecule Tracking. *Proc. Natl. Acad. Sci. U. S. A.* **2011**, *108*, 6438−6443.

(8) Ghosh, S. K.; Cherstvy, A. G.; Grebenkov, D. S.; Metzler, R. Anomalous, Non-Gaussian Tracer Diffusion in Crowded Two-Dimensional Environments. *New J. Phys.* **2016**, *18*, 013027.

(9) Chubynsky, M. V.; Slater, G. W. Diffusing Diffusivity: A Model for Anomalous, Yet Brownian, Diffusion. *Phys. Rev. Lett.* **2014**, *113*, 098302.

(10) Chechkin, A. V.; Seno, F.; Metzler, R.; Sokolov, I. M. Brownian Yet Non-Gaussian Diffusion: From Superstatistics to Subordination of Diffusing Diffusivities. *Phys. Rev. X* **2017**, *7*, 021002.

(11) Jain, R.; Sebastian, K. L. Diffusing Diffusivity: Fractional Brownian Oscillator Model for Subdiffusion and Its Solution. *Phys. Rev. E: Stat. Phys., Plasmas, Fluids, Relat. Interdiscip. Top.* **2018**, *98*, 052138.

(12) Palmieri, B.; Safran, S. A. Diffusion in a Soft Confining Environment: Dynamic Effects of Thermal Fluctuations. *Phys. Rev. E* **2012**, *86*, 031111.

(13) Marbach, S.; Dean, D. S.; Bocquet, L. Transport and Dispersion across Wiggling Nanopores. *Nat. Phys.* **2018**, *14*, 1108−1113.

(14) Li, Y.; Marchesoni, F.; Debnath, D.; Ghosh, P. K. Non-Gaussian Normal Diffusion in a Fluctuating Corrugated Channel. *Phys. Rev. Research* **2019**, *1*, 033003.

(15) Wong, I. Y.; Gardel, M. L.; Reichman, D. R.; Weeks, E. R.; Valentine, M. T.; Bausch, A. R.; Weitz, D. A. Anomalous Diffusion Probes Microstructure Dynamics of Entangled F-Actin Networks. *Phys. Rev. Lett.* **2004**, *92*, 178101.

(16) Lewis, J.; Sjostrom, J. Optimizing the Experimental Design of Soil Columns in Saturated and Unsaturated Transport Experiments. *J. Contam. Hydrol.* **2010**, *115*, 1−13.

(17) Vereecken, H.; Schnepf, A.; Hopmans, J.; Javaux, M.; Or, D.; Roose, T.; Vanderborght, J.; Young, M.; Amelung, W.; Aitkenhead, M.; Allison, S.; Assouline, S.; Baveye, P.; Berli, M.; Brüggemann, N.; Finke, P.; Flury, M.; Gaiser, T.; Govers, G.; Ghezzehei, T.; et al. Modeling Soil Processes: Review, Key Challenges, and New Perspectives. *Vadose Zone J.* **2016**, *15*, vzj2015.09.0131.

(18) Yang, S. Y.; Ryu, I.; Kim, H. Y.; Kim, J. K.; Jang, S. K.; Russell, T. P. Nanoporous Membranes with Ultrahigh Selectivity and Flux for the Filtration of Viruses. *Adv. Mater.* **2006**, *18*, 709−712.

(19) Berry, H.; Chaté, H. Anomalous Diffusion Due to Hindering by Mobile Obstacles Undergoing Brownian Motion or Orstein-Ulhenbeck Processes. *Phys. Rev. E* **2014**, *89*, 022708.

(20) Wu, H.; Sarfati, R.; Wang, D.; Schwartz, D. K. Electrostatic Barriers to Nanoparticle Accessibility of a Porous Matrix. *J. Am. Chem. Soc.* **2020**, *142*, 4696−4704.

(21) Miyaguchi, T. Reduction of Self-Diffusion Coefficient in a Coarse-Grained Model of Cytoplasm. *Phys. Rev. Research* **2020**, *2*, 013279.

(22) Eichmann, S. L.; Anekal, S. G.; Bevan, M. A. Electrostatically Confined Nanoparticle Interactions and Dynamics. *Langmuir* **2008**, *24*, 714−721.

(23) Habdas, P.; Schaar, D.; Levitt, A. C.; Weeks, E. R. Forced Motion of a Probe Particle near the Colloidal Glass Transition. *Europhysics Letters (EPL)* **2004**, *67*, 477−483.

(24) Grebenkov, D. S.; Oshanin, G. Diffusive Escape through a Narrow Opening: New Insights into a Classic Problem. *Phys. Chem. Chem. Phys.* **2017**, *19*, 2723−2739.

(25) Calderon, C. P. Motion Blur Filtering: A Statistical Approach for Extracting Confinement Forces and Diffusivity from a Single Blurred Trajectory. *Phys. Rev. E: Stat. Phys., Plasmas, Fluids, Relat. Interdiscip. Top.* **2016**, *93*, 053303.

(26) Dufresne, E. R.; Squires, T. M.; Brenner, M. P.; Grier, D. G. Hydrodynamic Coupling of Two Brownian Spheres to a Planar Surface. *Phys. Rev. Lett.* **2000**, *85*, 3317−3320.
(27) Skaug, M. J.; Wang, L.; Ding, Y.; Schwartz, D. K. Hindered Nanoparticle Diffusion and Void Accessibility in a Three-Dimensional Porous Medium. *ACS Nano* **2015**, *9*, 2148−2156.
(28) Yang, X.; Liu, C.; Li, Y.; Marchesoni, F.; Hänggi, P.; Zhang, H. P. Hydrodynamic and Entropic Effects on Colloidal Diffusion in Corrugated Channels. *Proc. Natl. Acad. Sci. U. S. A.* **2017**, *114*, 9564−9569.
(29) Merrill, J. W.; Sainis, S. K.; Bławzdziewicz, J.; Dufresne, E. R. Many-Body Force and Mobility Measurements in Colloidal Systems. *Soft Matter* **2010**, *6*, 2187−2192.
(30) Fernandes, G. E.; Beltran-Villegas, D. J.; Bevan, M. A. Spatially Controlled Reversible Colloidal Self-Assembly. *J. Chem. Phys.* **2009**, *131*, 134705.
(31) Crocker, J. C.; Grier, D. G. Methods of Digital Video Microscopy for Colloidal Studies. *J. Colloid Interface Sci.* **1996**, *179*, 298−310.

https://doi.org/10.1021/acsnano.1c00744
ACS Nano 2021, 15, 7392−7398